ACS Partner Journal

Journal of the American Society for Mass Spectrometry

pubs.acs.org/jasms

Article

Characterization of the Oxazolone and Macrocyclic Motifs in the b_n (n = 2−5) Product Ions from Collision-Induced Dissociation of Protonated Oligoglycine Peptides with Isomer-Selective, Cryogenic Vibrational Spectroscopy

Ahmed Mohamed, Abhijit Rana, Evan Perez, Franziska Dahlmann, Allison Fry, Fabian S. Menges, Michael van Stipdonk, Svenja Jäger, Mark A. Boyer, Anne B. McCoy, and Mark A. Johnson*

Cite This: *J. Am. Soc. Mass Spectrom.* 2024, 35, 326−332

Read Online

ACCESS | Metrics & More | Article Recommendations | Supporting Information

ABSTRACT: Collision-induced dissociation (CID) of small, protonated peptides leads to the formation of b-type fragment ions that can occur with several structural motifs driven by different covalent intramolecular bonding arrangements. Here, we characterize the so-called "oxazolone" and "macrocycle" $\mathbf{b}_n$ ion structures that occur upon CID of oligoglycine peptides (G_n) ions (n = 2−6). This is determined by acquiring the vibrational band patterns of the cryogenically cooled, D_2-tagged $\mathbf{b}_n$ ions obtained using isomer-selective, two-color IR−IR photobleaching and analyzing them with predicted (DFT) harmonic spectra for the candidate structures. Both oxazolone and macrocyclic isomers are formed by $\mathbf{b}_4$, whereas only oxazolone species are created for $\mathbf{b}_2$ and $\mathbf{b}_3$ and the macrocycle is created for $\mathbf{b}_5$. As such, n = 4 corresponds to the minimum size where both Oxa and MC forms are present.

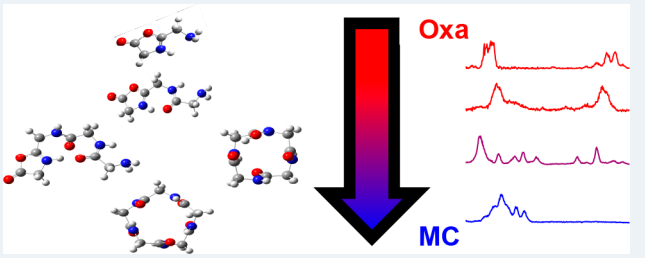

I. INTRODUCTION

The distribution of ions following collisional induced dissociation (CID) plays a central role in mass spectrometric analysis of complex mixtures ranging from the characterization of metabolites to sequencing peptides.[1] CID patterns are useful in providing information on the functional group presence and, in the case of peptides, sequence information through amino acid bond cleavage. However, there are situations in which an orthogonal analytical filter is useful to obtain more structural information and clarify the potential role of isomers. One such fragment is $\mathbf{b}_n$, obtained by fragmentation of protonated oligopeptides. Here, we focus on the simplest case of oligoglycine peptides (G_n) indicated in Figure 1. The $\mathbf{b}_n$ fragment forms by cleavage at the amide bond, leaving a positive charge on the side of the N-terminus. In favorable cases, this produces characteristic fragmentation patterns that can be used to determine the original peptide sequence. It is generally agreed that $\mathbf{b}_n$ ions are generated by a "mobile proton" mechanism. Internal energy supplied by collisions with buffer gas in the CID process forms reactive intermediates with protonation sites that lead to backbone dissociation.[2]

Protonation of the amide nitrogen in the G_n ions considerably weakens the amide bond, leading to decomposition.[3] Once the bond is weakened, the fragmentation pathway leading to $\mathbf{b}_n$ diverges, depending on the chain length of the peptide. The schemes of interest in this study are summarized in Schemes S1 and S2. The structures of the $\mathbf{b}_n$

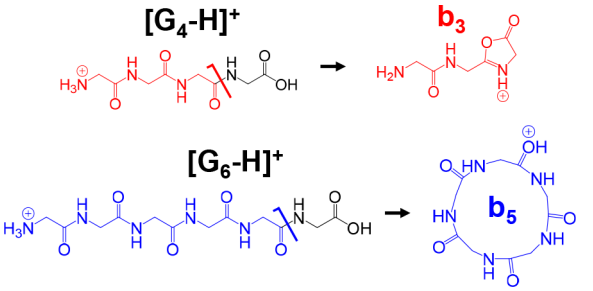

Figure 1. Product motifs adopted by the $\mathbf{b}_n$ fragments generated by the collisional dissociation of protonated oligoglycine peptides. Previous studies have reported two different structural classes generated depending on the number of glycine residues (n) in G_n. At small n, the oxazolone (Oxa, red) motif is the dominant form generated upon CID, whereas larger n precursors yield the macrocycle structure (MC, blue). Here, we exploit cryogenic vibrational spectroscopy to address how the distribution of the two forms evolves as a function of the number of n.

Received: October 23, 2023
Revised: November 30, 2023
Accepted: December 1, 2023
Published: December 27, 2023

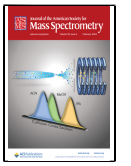

ions have been explored with vibrational spectroscopy using infrared multiple photon dissociation (IRMPD),[4−8] following the kinetics of H/D exchange (HDX),[9] and energy-resolved collision-induced dissociation.[10] For small polypeptides ($n \leq 3$), the $\mathbf{b}_n$ ions adopt the terminal oxazolone motif (hereafter denoted Oxa),[11,12] while the longer chains adopt the macrocycle form (hereafter denoted MC).[8,9] The nature of the $\mathbf{b}_n$ ion has practical implications because the MC isomer compromises the original sequence of the peptide, thus complicating sequencing based on the CID fragments.[13] Critical evaluations of the impact of this uncertainty on sequence identification have been carried out[14,15] and concluded that the overall effect is small at the MS/MS level (i.e., a single fragmentation step initiated with the protonated precursor peptide ion). Subsequent CID of putative macrocyclic isomers at the MS/MS/MS level and beyond has been shown to cause the scrambling of amino acid sequence.[8] Nonetheless, uncertainty remains about the *n*-dependence of the relative contributions of each isomer to the net $\mathbf{b}_n$ yield. This arises because previous studies reported portions of the IR spectrum (e.g., 800−2000 or 2500−4000 cm^{-1})[6,9,16] using IRMPD. Moreover, different laboratories necessarily generated CID products from different precursor ions with different CID methodologies (i.e., instrument-dependent commercial mass spec capabilities, break up in the ion source vs upon introduction to an RF trap).[6,9,15] We therefore undertook this study to determine the $\mathbf{b}_n$ structures generated by CID of G_n (n = 3−6) peptides with the widely used Thermo Fisher Scientific Orbitrap Velos Pro platform.

The $\mathbf{b}_n$ structures were determined by analysis of vibrational spectra of the cryogenically cooled, D_2-tagged ions over the spectral range 1000−3600 cm^{-1}. This approach features the advantage that vibrational band patterns reflect the linear absorption spectrum and are therefore directly comparable to calculated spectra for candidate structures recovered by electronic structure calculations. Moreover, isomer-specific spectra can be obtained using two-color IR−IR photobleaching to address the number of species contributing to each m/z ion packet as well as their highly resolved spectral signatures. We note that this work is an IR−IR variation of the earlier isomer-selective study of the $\mathbf{b}_4$ ion generated from the YGGFL[17] peptide sequence, which also focused on the cryogenically cooled ion using IR−UV bleaching. Those authors concluded that this $\mathbf{b}_4$ species exclusively adopted the Oxa motif, but a later study[6] carried out on room temperature ions using IRMPD raised the possibility that the calculated bands from the MC structure were in the best agreement with the observed spectra. Both ion spectroscopy studies[6,17] followed an earlier CID investigation of apparent sequence scrambling at the MS/MS/MS stage, in which compelling evidence that the onset for generation of macrocyclic ion structures is at $\mathbf{b}_4$.[18] The discrepancy in the IR photodissociation studies emphasizes the difficulty in comparing conclusions about the ion structure when different instruments, spectral regions, and fragmentation methods are used to record vibrational spectra. In light of this, we undertook this study to elucidate the *n*-dependence of the Oxa vs MC forms of the $\mathbf{b}_n$ ions created from a simple oligopeptide (G_n) under a consistent set of fragmentation conditions.

II. EXPERIMENTAL AND COMPUTATIONAL PROTOCOLS

The experimental methods and sample handling protocols have been described previously[19] and are presented in the Supporting Information. Briefly, ESI generated G_n ions (where *n* denotes the number of glycine residues which are charged by protonation) were subjected to collisional dissociation in the LTQ (linear trapping quadrupole) of the Thermo Fisher Scientific Orbitrap Velos Pro mass spectrometer. Fragmentation was carried out with a normalized collision energy of 30% and an activation time of 10 ms. A packet of ions held in the LTQ was transferred to an external, custom-built cryogenic ion trap held at 20 K. Ions were cooled and tagged with D_2 molecules seeded (25%) in the pulsed He buffer gas. After the buffer gas pressure was evacuated by effusion through the apertures in the trap for 95 ms, the ions were pulsed out of the cryogenic trap and into a triple-focusing photofragmentation time-of-flight mass spectrometer. Vibrational spectra were obtained by IR photodissociation (IRPD) of the D_2 tags using a standard LaserVision parametric converter (6 ns, Nd:YAG pumped KTP/KTA, OPO/OPA, extended to the 1000 to 2300 cm^{-1} range by nonlinear mixing in $AgGaSe_2$ described previously).[20] The laser was scanned over two partially overlapping spectral regions (1000 to 2300 cm^{-1} and 2200 to 3600 cm^{-1}) with different nonlinear mixing schemes. As a result, the spectra presented were merged together, such that the fragmentation intensities are matched at the overlap region. Isomer-selective spectra were acquired using two-color, IR−IR double resonance as described previously with details of its application here presented in the Supporting Information. To aid in the assignment of the spectra calculations were performed at the B3LYP/6-311+G(d,p) level of theory/basis using the Gaussian 16 program package.[21] Additional information about the approaches used in this work can be found in the Supporting Information.

III. RESULTS AND DISCUSSION

IIIA. Spectral Signature of the Oxazolone Motif.

Extensive studies using IRMPD and HDX on $\mathbf{b}_2$ fragments of protonated peptides have shown that these almost exclusively adopt the Oxa motif.[7,9,11,22] For example, Chen et al.[9] measured the infrared spectrum of $\mathbf{b}_2$ generated from triglycine in the fingerprint region and recovered the telltale CO stretching mode of the oxazolone structure at ∼1960 cm^{-1}. The high frequency region was measured by Wang et al. in a separate study.[12] Comparison of the NH and OH stretching bands with calculated candidate structures and the observed spectrum of cyclo(Gly-Gly) (the MC form of $\mathbf{b}_2$, also known as diketopiperazine) as a control confirmed that $\mathbf{b}_2$ from protonated triglycine exclusively forms Oxa. Moreover, this region of the spectrum allowed for assignment of the protonation site to the lactone ring, as opposed to the N-terminus. There are exceptions to exclusive Oxa formation in small b-type ions that have been known for decades with tandem MS/MS techniques.[23] One notable exception, which makes use of the diagnostic power of IR spectroscopy, to exclusive Oxa formation in $\mathbf{b}_2$ is in histidine-containing peptides in which MC and Oxa structures are both formed upon dissociation of the precursor peptide ion, HAAAA.[24]

To establish the spectral features that confirm the formation of Oxa structures in the cryogenic vibrational spectra, Figure 2 presents the D_2-tagged spectra of the $\mathbf{b}_2$ and $\mathbf{b}_3$ ions. The

https://doi.org/10.1021/jasms.3c00372
J. Am. Soc. Mass Spectrom. 2024, 35, 326−332

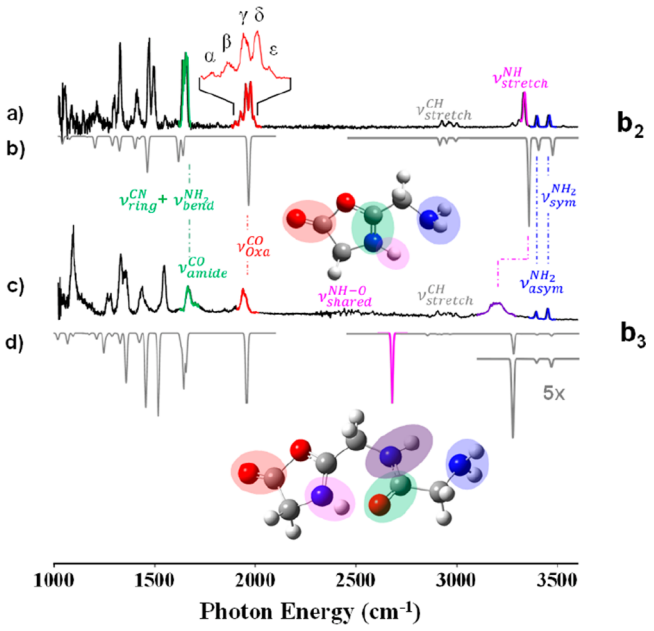

Figure 2. (a, c) D_2-tagged IRPD spectra of $\mathbf{b_2}$ and $\mathbf{b_3}$. Inverted scaled harmonic spectra and structures are presented for the ring-protonated (Oxa) $\mathbf{b_2}$ (b) and $\mathbf{b_3}$ (d) ions predicted at the B3LYP/6-311+G(d,p) level of theory. The computed spectra are scaled by 0.96 in the range of 2400−3600 cm^{-1} to match the NH_2 symmetric and asymmetric stretches and 0.975 in the range of 1000−2100 cm^{-1} to match the lactone CO of Oxa. The expanded inset in (a) highlights the multiplet structure displayed by the experimental spectrum of $\mathbf{b_2}$, whereas only a single feature is predicted in the region arising from the CO stretching fundamental. Energies of selected bands are listed in Table S1. The high frequency region in (d) has been expanded to highlight the relative intensities of the NH_2 fundamentals.

experimental spectrum of $\mathbf{b_2}$ is shown in Figure 2a. The observed spectrum displays a multiplet centered at 1962 cm^{-1} (highlighted in red), which has been assigned previously to the CO stretching fundamental of the carbonyl group and denoted ν^{CO}_{Oxa}.[25] In the cold ion spectrum, however, the broad CO envelope observed in the IRMPD spectrum is resolved into a quintet of closely spaced peaks separated by about 20 cm^{-1}. This behavior is not predicted at the harmonic level (Figure 2b), which displays only a single, isolated transition in this region. Therefore, it is likely that the multiplet is due to anharmonic coupling with background states. Indeed, calculations performed using second-order vibrational perturbation theory (VPT2) show several closely spaced peaks in this region (Figure S1c). The $\mathbf{b_2}$ ion retains its N-terminus $-NH_2$ motif, as evidenced by the symmetric ($\nu^{NH_2}_{sym}$) and asymmetric ($\nu^{NH_2}_{asym}$) modes at 3390 and 3454 cm^{-1}, respectively (highlighted in blue), along with a strong band just below them at 3329 cm^{-1}. All of these features are recovered at the harmonic level (Figure 2b), verifying that the 3329 cm^{-1} band arises from the ring NH group. Although previous spectroscopic studies have observed Oxa containing ion ensembles with different protonation sites (ring-protonated vs N-terminal-protonated),[5] this possibility is discounted here as the high frequency region of the spectrum (Figure 2a) exclusively contains bands associated with neutral $-NH_2$. As such, the observed multiplet of ν^{CO}_{Oxa} is not related to species involving protonation of the N-terminus. There is the possibility of subtle isomer effects which can be addressed with IR−IR photobleaching techniques as described in the experimental protocol; however, this lies outside the scope of the present study.

The D_2-tagged spectrum of $\mathbf{b_3}$ is displayed in Figure 2c, which also contains the telltale ν^{CO}_{Oxa} peak at 1941 cm^{-1}, confirming the formation of the Oxa motif. Although the quintet structure of the ν^{CO}_{Oxa} band observed in the $\mathbf{b_2}$ spectrum is not found in $\mathbf{b_3}$, the band contour shows a similar overall envelope to that seen in $\mathbf{b_2}$. The $\nu^{NH_2}_{sym}$ and $\nu^{NH_2}_{asym}$ features of the $-NH_2$ group are intact (blue), but there is a strong, broad feature present in the NH stretching region (purple) centered at 3200 cm^{-1}. This is red-shifted by 130 cm^{-1} from the location of a free NH group in that position of $\mathbf{b_2}$, and we assign this feature to the NH group engaged in a five-membered cyclic structure with an intramolecular H-bond, which is in accordance with the spectrum calculated (inverted in Figure 2d) for the structure displayed in the inset of Figure 2d. The broadening associated with such cyclic intramolecular H-bonds has been reported for many systems.[26] Such broadening can become extreme as the strength of the H-bond increases along with the red-shift. Indeed, in prototype systems with red-shifts on the order of 800 cm^{-1}, the envelope of the oscillator strength is difficult to observe with linear spectroscopy.[27] The calculated shift (700 cm^{-1}, pink peak in Figure 2d) associated with the second NH is such a case. It is also engaged in a cyclic intramolecular H-bond (this time a seven-membered ring), and we therefore conclude that this band is not recovered at the current signal-to-noise ratio.

Figure 3 presents the experimental D_2-tagged spectra of the $\mathbf{b}_{n=2-5}$ series. Cursory inspection of the band patterns indicates

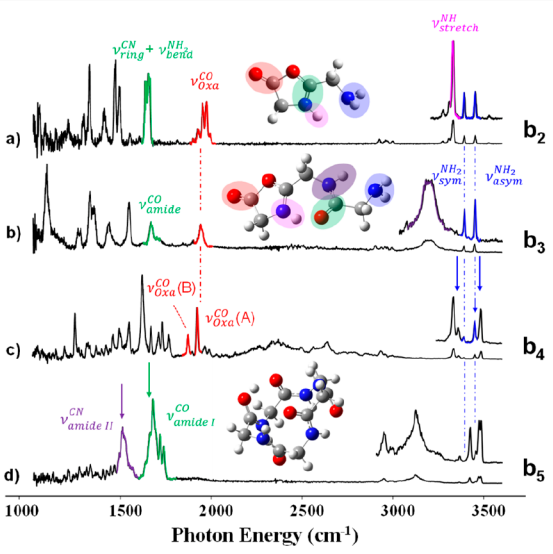

Figure 3. D_2-tagged IRPD spectra of $\mathbf{b}_n$ for n = (a) 2, (b) 3, (c) 4, and (d) 5. Expanded insets of the high frequency region are shown to illustrate the evolution of the NH_2 fundamentals, as well as transitions arising from the NH stretch. The blue arrows in (c) represent the frequencies of $\mathbf{b_4}$ measured previously by Durand et al.[6] The purple and green arrows in (d) represent the frequencies of $\mathbf{b_5}$ measured previously by Erlekam et al.[16] All minimum energy structures shown as insets were calculated at the B3LYP/6-311+G(d,p) level of theory.

that, while the $\mathbf{b_4}$ spectrum retains the signature CO stretch (ν^{CO}_{Oxa}(A)), red at 1927 cm^{-1}), this feature is completely absent in the spectrum of $\mathbf{b_5}$ (Figure 3d). There is a broad pedestal that spans the location of the ν^{CO}_{Oxa} band, but this continuum envelope is inconsistent with that expected for a nonbonded

https://doi.org/10.1021/jasms.3c00372
J. Am. Soc. Mass Spectrom. 2024, 35, 326−332

CO group in the Oxa motif. The observed behavior is expected based on a previous report that the MC isomer is exclusively formed upon CID of Gly-Gly-Gly-Gly-Gly-Arg (G_5R).[16] That conclusion was based on the IRMPD spectrum that featured two broad bands (purple and green arrows in Figure 3d) centered at 1520 and 1680 cm^{-1}. These are expected for the amide II (CN stretch, ($\nu^{CN}_{amide\ II}$), purple arrow) and amide I (CO stretch, ($\nu^{CO}_{amide\ I}$), green arrow) modes of a polypeptide, respectively.[28] A pattern similar to that for the D_2-tagged $\mathbf{b_5}$ ion is observed here (Figure 3d). Moreover, within the macrocyclic structure, all of the nitrogen atoms are secondary and appear with one NH group. As a result, the characteristic $\nu^{NH_2}_{sym}$ and $\nu^{NH_2}_{asym}$ bands of the N-terminus (blue dashed vertical lines in Figure 3) are not present in the observed $\mathbf{b_5}$ spectrum. Instead, these are replaced by a multiplet of transitions in the region from ~3300 to 3500 cm^{-1}. Based on this spectral behavior, we conclude that the $\mathbf{b_5}$ ion created in this work starting from G_6 also occurs exclusively in the MC motif. We note that this is in contrast with the situation reported for the $\mathbf{b_5}$ ion generated from G_8. In that case, features in the IRMPD spectrum, as well as the HDX kinetics, pointed to a scenario in which both Oxa and MC were in play.[9] The method of CID used in that study[9] (nozzle-skimmer breakup) was different from that used for G_5R[16] and G_6 (ion trap), raising the possibility that different kinetic regimes can control the final $\mathbf{b_5}$ ion structure.

Returning to the $\mathbf{b_4}$ spectrum (Figure 3c), we note that it is qualitatively more complex than the others with many distinct bands scattered across the entire spectrum as well as a very broad feature centered at 2500 cm^{-1} signaling the presence of a strong H-bond. As discussed above, the $\nu^{CO}_{Oxa}(A)$ feature at 1926 cm^{-1} provides compelling evidence that the Oxa motif is present, and this is further confirmed by the high frequency NH region, which yields sharp bands at locations of the $\nu^{NH_2}_{sym}$ and $\nu^{NH_2}_{asym}$ stretches (dotted blue lines at 3392 and 3452 cm^{-1}, respectively). These bands do not occur with the same intensity ratio as $\mathbf{b_2}$ and $\mathbf{b_3}$; however, many other features appear nearby including very strong transitions at 3338 and 3486 cm^{-1}. The band locations indicated by the downward blue arrows in Figure 3c correspond to those obtained for the room temperature $\mathbf{b_4}$ ions (from G_5) using a two-color technique: a resonant IR pulse followed by IRMPD with a CO_2 laser.[6] Those authors found this pattern to be most consistent with the exclusive formation of the Oxa form. On the other hand, HDX data on $\mathbf{b_4}$ (again from G_5) reported by Chen et al.[9] indicated that two species were present that are consistent with the occurrence of both Oxa and MC forms. Even in the context of the Oxa structure, the observed spectrum displays an isolated band at 1876 cm^{-1} ($\nu^{CO}_{Oxa}(B)$), ~50 cm^{-1} below the $\nu^{CO}_{Oxa}(A)$ feature. This suggests the formation of a second oxazolone-based isomer. To establish the number of isomers that contribute to the $\mathbf{b_4}$ spectrum, we extended the study of the $\mathbf{b_4}$ ion ensemble prepared in our ion source using isomer-selective, two-color IR−IR spectroscopy.

IIIB. Isomer-Selective Spectra of $\mathbf{b_4}$. Isomer-selective IRPD is achieved using two pulsed (6 ns) IR lasers, with one of them (the pump) fixed on a particular transition in the single laser spectrum and sufficiently powerful to remove a significant fraction of the ion population of the species with a band resonant with the pump frequency. A second laser (the probe) subsequently interrogates the same ion packet excited by the pump laser and is scanned across the entire spectrum. All transitions associated with the species excited by the pump are then recorded by monitoring the degree to which the photofragment from the probe is modulated by the pump, which is pulsed over alternate cycles of the 5 Hz experiment.

We first consider the nature of the species responsible for the $\nu^{CO}_{Oxa}(A)$ feature in the $\mathbf{b_4}$ single laser spectrum reproduced in Figure 4c. That band appears closest to the telltale

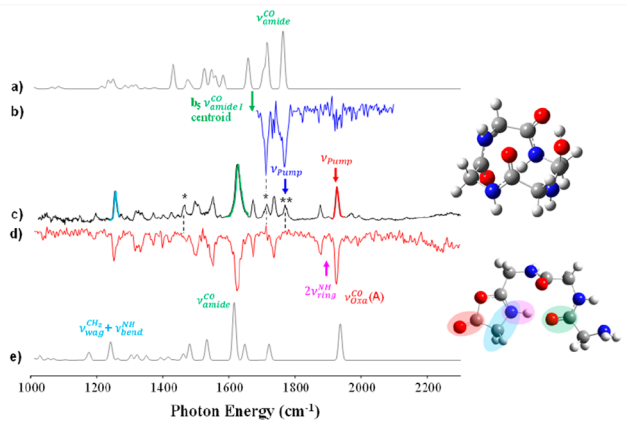

Figure 4. (a) Harmonic (B3LYP/6-311+G(d,p)) spectrum (scaled by 0.975) for the O-protonated MC structure shown in the inset. (b) Isomer-specific spectrum of $\mathbf{b_4}$ with the pump laser located at the band indicated by the blue downward arrow (ν_{Pump}). The green downward arrow indicates the centroid frequency of $\nu^{CO}_{amide\ I}$ in $\mathbf{b_5}$. (c) D_2-tagged IRPD spectrum of $\mathbf{b_4}$, (d) isomer-specific spectrum obtained with the pump located at the $\nu^{CO}_{Oxa}(A)$ band (red arrow), and (e) harmonic (B3LYP/6-311+G(d,p)) spectrum (scaled by 0.975) for the ring-protonated structure shown in the inset. The pink arrow in (d) indicates the calculated position of the ν = 0−2 transition of the bending mode arising from the H-bonded NH stretch on the oxazolone ring ($2\nu^{NH}_{ring}$, pink). See the text and Figure S2 for details on the anharmonic vibrational calculations and analysis of $\mathbf{b_4}$.

transitions in the $\mathbf{b_2}$ and $\mathbf{b_3}$ spectra, signaling formation of the Oxa motif. Setting the pump laser to the $\nu^{CO}_{Oxa}(A)$ feature yields the modulated spectrum displayed in Figure 4d (red, where negative going modulations indicate signals that are reduced when the pump laser is on). Several key points are immediately established by comparing the two spectra. First, three strong bands in the single laser spectrum (indicated by asterisks) are missing in the isomer-selective trace, thus establishing that there are at least two spectroscopically distinct species in play. Second, both bands in the vicinity of the Oxa CO stretch [$\nu^{CO}_{Oxa}(A)$ and $\nu^{CO}_{Oxa}(B)$] are modulated when the pump is fixed on $\nu^{CO}_{Oxa}(A)$, indicating that these bands arise from the same isomer. With the exception of the $\nu^{CO}_{Oxa}(B)$ transition, the pattern of bands is accurately recovered at the (scaled) harmonic level for the Oxa structure presented in the inset in Figure 4e. This agreement indicates that the dominant band near 1600 cm^{-1} is due to the terminal amide CO vibrational mode, with a few other key bands labeled according to the dominant displacements in the calculated normal modes. Note that this structure also rationalizes the very diffuse envelope that extends from 2000 to 2500 cm^{-1} due to the ring NH group (Figure 4e, pink) attached to the terminal amide CO group.

To explore the origin of the $\nu^{CO}_{Oxa}(B)$ band, we carried out anharmonic calculations (VPT2) also at the B3LYP/6-311+G(d,p) level of theory/basis to capture overtone and combination bands predicted to gain oscillator strength in this

https://doi.org/10.1021/jasms.3c00372
J. Am. Soc. Mass Spectrom. 2024, 35, 326−332

region. The anharmonic spectrum is presented in Figure S2, and indeed a band close to ν_{Oxa}^{CO}(B) is predicted (pink upward arrow in Figure 4d), which arises from the overtone of the bending mode associated with the NH group engaged in a H-bond to the CO ($2\nu_{ring}^{NH}$). This effect has been observed in many systems[29,30] and occurs when soft mode displacements (normal mode vectors indicated in the inset of Figure S2d) act to break the strong H-bond. Analagous bands are also found in the calculated anharmonic spectra for $\mathbf{b}_2$ (1451 cm^{-1}) and $\mathbf{b}_3$ (1935 cm^{-1}).

The spectrum of the second $\mathbf{b}_4$ isomer is displayed in Figure 4b (blue trace with downward features associated with population depletion). This spectrum was isolated by setting the pump laser at the highest energy feature in the single laser spectrum that is not associated with the Oxa isomer, indicated by the blue arrow in Figure 4a at 1767 cm^{-1}. The neighboring (*) band at 1715 cm^{-1} is also modulated by this pump frequency, whereas there is no activity near the ν_{Oxa}^{CO}(A) and (B) bands assigned to the spectrum of the Oxa isomer. We therefore conclude that the second isomer does not adopt the oxazolone motif. The strong doublet structure of the highest energy bands in the fingerprint region is in excellent agreement with the calculated (scaled) harmonic calculation presented in Figure 4a for the lowest energy MC structure depicted in the inset. These two strong bands arise from the CO stretches of the polyamide scaffold. We note that the relatively weak laser power in this spectral region required extensive signal averaging, and here, we establish only the necessary differences in the spectra of the two isomers. More extensive experimental work will be required if a complete survey of the entire spectrum is desired to better resolve the actual structure of the MC species. We note that the MC structural motif was calculated by Paizs and co-workers to be 3.5 kcal/mol above the ring-protonated Oxa structure,[6] supporting the role of kinetic quenching into local minima in the complex potential energy landscape. In the present study, a similar difference in energy and preference for the Oxa structure were predicted with the B3LYP functional. However, calculations at the M06-2X and MP2 levels of theory predicted the MC and Oxa structures to be nearly isoenergetic, which supports the observation of multiple isomers for the b_4 ion population generated by CID of G_4 in our study, as suggested in previous reports.[18,31]

These results establish that the $\mathbf{b}_4$ ion generated from G_5 under our dissociation conditions occurs in both Oxa and MC forms, and thus corresponds to an effective "tipping point" in the transition from exclusive formation of Oxa structures for smaller sizes and MC structures for midsized precursor G_n peptides.

IV. SUMMARY

Isomer-selective cryogenic ion vibrational spectroscopy and quantum chemical calculations unambiguously identify two isomer forms of the $\mathbf{b}_4$ fragment. One of these corresponds to the oxazolone motif reported earlier, but a second structure is also observed that corresponds to formation of a macrocycle. The CO stretch near 1926 cm^{-1}, the telltale feature of the oxazolone isomer, appears with another strong band at 1876 cm^{-1}. Double-resonance spectra based on isomer-selective photobleaching confirm that both bands arise from the same species, ruling out the formation of different oxazolone conformers. Anharmonic calculations suggest the 1876 cm^{-1} band is associated with an overtone transition involving the out-of-plane motion of an NH group, which breaks the NH···O hydrogen bond. The $\mathbf{b}_2$ and $\mathbf{b}_3$ fragments exclusively adopt the oxazolone structure in agreement with previous studies, but only the macrocyclic form of the $\mathbf{b}_5$ ion is present. This result differs from an earlier conclusion based on IRMPD and HDX kinetics that $\mathbf{b}_5$ exists in both macrocyclic and oxazolone forms and raises the important question of how the $\mathbf{b}_n$ structures depend on the specific CID protocols used, as well as the issue of how fragment ions with significant internal energy are quenched into different minima upon cryogenic cooling.

■ ASSOCIATED CONTENT

Supporting Information

The Supporting Information is available free of charge at https://pubs.acs.org/doi/10.1021/jasms.3c00372.

Experimental methods, computational methods, and calculated anharmonic spectra (PDF)

■ AUTHOR INFORMATION

Corresponding Author

Mark A. Johnson − *Sterling Chemistry Laboratory, Department of Chemistry, Yale University, New Haven, Connecticut 06520, United States;* orcid.org/0000-0002-1492-6993; Email: mark.johnson@yale.edu

Authors

Ahmed Mohamed − *Sterling Chemistry Laboratory, Department of Chemistry, Yale University, New Haven, Connecticut 06520, United States*

Abhijit Rana − *Sterling Chemistry Laboratory, Department of Chemistry, Yale University, New Haven, Connecticut 06520, United States*

Evan Perez − *Sterling Chemistry Laboratory, Department of Chemistry, Yale University, New Haven, Connecticut 06520, United States; The University of Utah, Salt Lake City, Utah 84112, United States*

Franziska Dahlmann − *Institut for Ion Physics and Applied Physics, University of Innsbruck, 6020 Innsbruck, Austria;* orcid.org/0000-0003-2898-7460

Allison Fry − *Center of Excellence in Mass Spectrometry, Center for Metal Ions in Biological and Chemical Systems, Department of Chemistry and Biochemistry, Duquesne University, Pittsburgh, Pennsylvania 15282, United States*

Fabian S. Menges − *Sterling Chemistry Laboratory, Department of Chemistry, Yale University, New Haven, Connecticut 06520, United States;* orcid.org/0000-0002-5859-9197

Michael van Stipdonk − *Center of Excellence in Mass Spectrometry, Center for Metal Ions in Biological and Chemical Systems, Department of Chemistry and Biochemistry, Duquesne University, Pittsburgh, Pennsylvania 15282, United States;* orcid.org/0000-0002-7100-4370

Svenja Jäger − *Chair of Physical Chemistry II, Ruhr-University Bochum, 44801 Bochum, Germany*

Mark A. Boyer − *Department of Chemistry, University of Wisconsin-Madison, Madison, Wisconsin 53706, United States*

Anne B. McCoy − *Department of Chemistry, University of Washington, Seattle, Washington 98195, United States;* orcid.org/0000-0001-6851-6634

Complete contact information is available at: https://pubs.acs.org/10.1021/jasms.3c00372

Author Contributions

A.M., A.R., S.J., and F.D. performed the cryogenic IR spectroscopy experiments. M.v.S., A.F., and A.B.M. performed the quantum chemical calculations. M.A.B. and A.B.M. performed the vibrational perturbation theory calculations. M.v.S. and E.P. designed the research. M.v.S. and M.A.J. supervised the research. All authors analyzed the data and interpreted the results. A.M. and M.A.J. wrote the manuscript. F.S.M. constructed and maintained the complex instrumentation used in these measurements.

Notes

The authors declare no competing financial interest.

■ ACKNOWLEDGMENTS

M.A.J. thanks the Air Force Office of Scientific Research for support of this work, which was started under grant FA9550-18-1-0213 and continued under MURI grant 62742085-204669 in the context of quantifying structures generated by collisional dissociation of precursor ions. The laser equipment essential to this work was optimized through the efforts of Dr. Tim Schleif. F.D. was supported by the Austrian Science Fund (FWF) (Project No. I2920-N27) and the Doctoral Program Atoms, Light and Molecules (Project No. W1259-N27). A.M. thanks the National Institutes of Health for support through the Predoctoral Program in Biophysics T32 GM008283. Research reported in this publication was also supported by the National Institute of General Medical Sciences of the National Institutes of Health under award number 5T32GM067543-20. A.B.M. thanks the National Science Foundation under grant NSF-CHE-2154126. A.F. and M.v.S. acknowledge support from the National Science Foundation (CHE-1726824) and the Robert Dean Loughney Faculty Development Endowment of Duquesne University.

■ REFERENCES

(1) Zhang, Y.; Fonslow, B. R.; Shan, B.; Baek, M. C.; Yates, J. R., 3rd Protein analysis by shotgun/bottom-up proteomics. *Chem. Rev.* **2013**, *113* (4), 2343−94.

(2) Paizs, B.; Suhai, S. Fragmentation pathways of protonated peptides. *Mass Spectrom Rev.* **2005**, *24* (4), 508−548.

(3) McCormack, A. L.; Somogyi, A.; Dongré, A. R.; Wysocki, V. H. Fragmentation of protonated peptides: surface-induced dissociation in conjunction with a quantum mechanical approach. *Anal. Chem.* **1993**, *65* (20), 2859−72.

(4) Wang, D.; Gulyuz, K.; Stedwell, C. N.; Polfer, N. C. Diagnostic NH and OH vibrations for oxazolone and diketopiperazine structures: b2 from protonated triglycine. *J. Am. Soc. Mass Spectrom.* **2011**, *22* (7), 1197−203.

(5) Polfer, N. C.; Oomens, J.; Suhai, S.; Paizs, B. Infrared Spectroscopy and Theoretical Studies on Gas-phase Protonated Leu-enkephalin and its Fragments: Direct experimental evidence for the mobile proton. *J. Am. Chem. Soc.* **2007**, *129* (18), 5887−5897.

(6) Durand, S.; Rossa, M.; Hernandez, O.; Paizs, B.; Maître, P. IR Spectroscopy of b4 Fragment Ions of Protonated Pentapeptides in the X−H (X = C, N, O) Region. *J. Phys. Chem. A* **2013**, *117* (12), 2508−2516.

(7) Oomens, J.; Young, S.; Molesworth, S.; van Stipdonk, M. Spectroscopic evidence for an oxazolone structure of the b2 fragment ion from protonated tri-alanine. *J. Am. Soc. Mass Spectrom.* **2009**, *20* (2), 334−339.

(8) Bleiholder, C.; Osburn, S.; Williams, T. D.; Suhai, S.; Van Stipdonk, M.; Harrison, A. G.; Paizs, B. Sequence-Scrambling Fragmentation Pathways of Protonated Peptides. *J. Am. Chem. Soc.* **2008**, *130* (52), 17774−17789.

(9) Chen, X.; Yu, L.; Steill, J. D.; Oomens, J.; Polfer, N. C. Effect of Peptide Fragment Size on the Propensity of Cyclization in Collision-Induced Dissociation: Oligoglycine b_2-b_8. *J. Am. Chem. Soc.* **2009**, *131* (51), 18272−18282.

(10) Armentrout, P. B.; Clark, A. A. The simplest b2+ ion: Determining its structure from its energetics by a direct comparison of the threshold collision-induced dissociation of protonated oxazolone and diketopiperazine. *Int. J. Mass Spectrom.* **2012**, *316-318*, 182−191.

(11) Chen, X.; Steill, J. D.; Oomens, J.; Polfer, N. C. Oxazolone Versus Macrocycle Structures for Leu-Enkephalin b(2)-b(4): Insights from Infrared Multiple-Photon Dissociation Spectroscopy and Gas-Phase Hydrogen/Deuterium Exchange. *J. Am. Soc. Mass Spectrom.* **2010**, *21* (8), 1313−1321.

(12) Wang, D.; Gulyuz, K.; Stedwell, C. N.; Polfer, N. C. Diagnostic NH and OH Vibrations for Oxazolone and Diketopiperazine Structures: b_2 from Protonated Triglycine. *J. Am. Soc. Mass Spectrom.* **2011**, *22* (7), 1197−1203.

(13) Harrison, A. G.; Young, A. B.; Bleiholder, C.; Suhai, S.; Paizs, B. Scrambling of Sequence Information in Collision-Induced Dissociation of Peptides. *J. Am. Chem. Soc.* **2006**, *128* (32), 10364−10365.

(14) Saminathan, I. S.; Wang, X. S.; Guo, Y.; Krakovska, O.; Voisin, S.; Hopkinson, A. C.; Siu, K. W. M. The extent and effects of peptide sequence scrambling via formation of macrocyclic b ions in model proteins. *J. Am. Soc. Mass Spectrom.* **2010**, *21* (12), 2085−2094.

(15) Goloborodko, A. A.; Gorshkov, M. V.; Good, D. M.; Zubarev, R. A. Sequence Scrambling in Shotgun Proteomics is Negligible. *J. Am. Soc. Mass Spectrom.* **2011**, *22* (7), 1121−1124.

(16) Erlekam, U.; Bythell, B. J.; Scuderi, D.; Van Stipdonk, M.; Paizs, B.; Maitre, P. Infrared Spectroscopy of Fragments of Protonated Peptides: Direct Evidence for Macrocyclic Structures of b(5) Ions. *J. Am. Chem. Soc.* **2009**, *131* (32), 11503−11508.

(17) Wassermann, T. N.; Boyarkin, O. V.; Paizs, B.; Rizzo, T. R. Conformation-Specific Spectroscopy of Peptide Fragment Ions in a Low-Temperature Ion Trap. *J. Am. Soc. Mass Spectrom.* **2012**, *23* (6), 1029−1045.

(18) Molesworth, S.; Osburn, S.; Van Stipdonk, M. Influence of size on apparent scrambling of sequence during CID of b-type ions. *J. Am. Soc. Mass Spectrom.* **2009**, *20* (11), 2174−2181.

(19) Menges, F. S.; Perez, E. H.; Edington, S. C.; Duong, C. H.; Yang, N.; Johnson, M. A. Integration of High-Resolution Mass Spectrometry with Cryogenic Ion Vibrational Spectroscopy. *J. Am. Soc. Mass Spectrom.* **2019**, *30* (9), 1551−1557.

(20) Wolk, A. B.; Leavitt, C. M.; Garand, E.; Johnson, M. A. Cryogenic Ion Chemistry and Spectroscopy. *Acc. Chem. Res.* **2014**, *47* (1), 202−210.

(21) Frisch, M. J.; Trucks, G. W.; Schlegel, H. B.; Scuseria, G. E.; Robb, M. A.; Cheeseman, J. R.; Scalmani, G.; Barone, V.; Petersson, G. A.; Nakatsuji, H.; Li, X.; Caricato, M.; Marenich, A. V.; Bloino, J.; Janesko, B. G.; Gomperts, R.; Mennucci, B.; Hratchian, H. P.; Ortiz, J. V.; Izmaylov, A. F.; Sonnenberg, J. L.; Williams; Ding, F.; Lipparini, F.; Egidi, F.; Goings, J.; Peng, B.; Petrone, A.; Henderson, T.; Ranasinghe, D.; Zakrzewski, V. G.; Gao, J.; Rega, N.; Zheng, G.; Liang, W.; Hada, M.; Ehara, M.; Toyota, K.; Fukuda, R.; Hasegawa, J.; Ishida, M.; Nakajima, T.; Honda, Y.; Kitao, O.; Nakai, H.; Vreven, T.; Throssell, K.; Montgomery, J. A., Jr.; Peralta, J. E.; Ogliaro, F.; Bearpark, M. J.; Heyd, J. J.; Brothers, E. N.; Kudin, K. N.; Staroverov, V. N.; Keith, T. A.; Kobayashi, R.; Normand, J.; Raghavachari, K.; Rendell, A. P.; Burant, J. C.; Iyengar, S. S.; Tomasi, J.; Cossi, M.; Millam, J. M.; Klene, M.; Adamo, C.; Cammi, R.; Ochterski, J. W.; Martin, R. L.; Morokuma, K.; Farkas, O.; Foresman, J. B.; Fox, D. J. *Gaussian 16*, Rev. B.01; Gaussian, Inc.: Wallingford, CT, 2016.

(22) Yoon, S. H.; Chamot-Rooke, J.; Perkins, B. R.; Hilderbrand, A. E.; Poutsma, J. C.; Wysocki, V. H. IRMPD Spectroscopy Shows That AGG Forms an Oxazolone b2+ Ion. *J. Am. Chem. Soc.* **2008**, *130* (52), 17644−17645.

(23) Farrugia, J. M.; Taverner, T.; O'Hair, R. A. J. Side-chain involvement in the fragmentation reactions of the protonated methyl esters of histidine and its peptides††Part 30 of the series "Gas Phase

https://doi.org/10.1021/jasms.3c00372
J. Am. Soc. Mass Spectrom. 2024, 35, 326−332

Ion Chemistry of Biomolecules. *Int. J. Mass Spectrom.* **2001**, *209* (2), 99−112.
(24) Perkins, B. R.; Chamot-Rooke, J.; Yoon, S. H.; Gucinski, A. C.; Somogyi, Á.; Wysocki, V. H. Evidence of Diketopiperazine and Oxazolone Structures for HA b2+ Ion. *J. Am. Chem. Soc.* **2009**, *131* (48), 17528−17529.
(25) Polfer, N. C.; Oomens, J.; Suhai, S.; Paizs, B. Spectroscopic and Theoretical Evidence for Oxazolone Ring Formation in Collision-Induced Dissociation of Peptides. *J. Am. Chem. Soc.* **2005**, *127* (49), 17154−17155.
(26) Leavitt, C. M.; DeBlase, A. F.; van Stipdonk, M.; McCoy, A. B.; Johnson, M. A. Hiding in Plain Sight: Unmasking the Diffuse Spectral Signatures of the Protonated N-Terminus in Simple Peptides. *J. Phys. Chem. Lett.* **2013**, *4*, 3450−3457.
(27) Johnson, C. J.; Dzugan, L. C.; Wolk, A. B.; Leavitt, C. M.; Fournier, J. A.; McCoy, A. B.; Johnson, M. A. Microhydration of Contact Ion Pairs in $M^{2+}O\bar{H}(H_2O)_{n=1-5}$ (M = Mg, Ca) Clusters: Spectral Manifestations of a Mobile Proton Defect in the First Hydration Shell. *J. Phys. Chem. A* **2014**, *118* (35), 7590−7597.
(28) Bandekar, J. Amide modes and protein conformation. *Biochimica et Biophysica Acta (BBA) - Protein Structure and Molecular Enzymology* **1992**, *1120* (2), 123−143.
(29) Stropoli, S. J.; Khuu, T.; Boyer, M. A.; Karimova, N. V.; Gavin-Hanner, C. F.; Mitra, S.; Lachowicz, A. L.; Yang, N.; Gerber, R. B.; McCoy, A. B.; Johnson, M. A. Electronic and mechanical anharmonicities in the vibrational spectra of the H-bonded, cryogenically cooled X- center dot HOCl (X = Cl, Br, I) complexes: Characterization of the strong anionic H-bond to an acidic OH group. *J. Chem. Phys.* **2022**, *156* (17), 174303.
(30) Roscioli, J. R.; Diken, E. G.; Johnson, M. A.; Horvath, S.; McCoy, A. B. Prying Apart a Water Molecule with Anionic H-Bonding: A Comparative Spectroscopic Study of the $X{\cdot}H_2O$ (X = OH, O, F, Cl, and Br) Binary Complexes in the 600−3800 cm^{-1} Region. *J. Phys. Chem. A* **2006**, *110* (15), 4943−4952.
(31) Gucinski, A. C.; Somogyi, S.; Chamot-Rooke, J.; Wysocki, V. H. Separation and Identification of Structural Isomers by Quadrupole Collision-Induced Dissociation-Hydrogen/Deuterium Exchange-Infrared Multiphoton Dissociation (QCID-HDX-IRMPD). *J. Am. Soc. Mass Spectrom.* **2010**, *21*, 1329−1338.

https://doi.org/10.1021/jasms.3c00372
J. Am. Soc. Mass Spectrom. 2024, 35, 326−332